arXiv:cond-mat/0403489v1 [cond-mat.soft] 19 Mar 2004

Anisotropy driven dynamics in vibrated granular rods

Dmitri Volfson[1], Arshad Kudrolli[2] and Lev S. Tsimring[1]
[1] *Institute for Nonlinear Science, University of California, San Diego, La Jolla, CA 92093-0402*
[2] *Department of Physics, Clark University, MA 01610*
(Dated: March 22, 2022)

The dynamics of a set of rods bouncing on a vertically vibrated plate is investigated using experiments, simulations, and theoretical analysis. The experiments and simulations are performed within an annulus to impose periodic boundary conditions. Rods tilted with respect to the vertical are observed to spontaneously develop a horizontal velocity depending on the acceleration of the plate. For high plate acceleration, the rods are observed to always move in the direction of tilt. However, the rods are also observed to move opposite to direction of tilt for a small range of plate acceleration and rod tilt. A phase diagram of the observed motion is presented as a function of plate acceleration and the tilt of the rods which is varied by changing the number of rods inside the annulus. Next we introduce a novel molecular dynamics method to simulate the dynamics of the rods using the dimensions and dissipation parameters from the experiments. We reproduce the observed horizontal rod speeds as a function of rod tilt and plate acceleration in the simulations. By decreasing the friction between the rods and the base plate to zero in the simulation, we identify the friction during the collision as the crucial ingredient for occurrence of the horizontal motion. Guided by the data from the experiments and the simulations, we construct a mechanical model for the dynamics of the rods in the limit of thin rods. The starting point of the analysis is the collision of a single rod with an oscillating plate. Three friction regimes are identified: slide, slip-stick, and slip reversal. A formula is derived for the observed horizontal velocity as a function of tilt angle. Good agreement for the horizontal velocity as a function of rod tilt and plate acceleration is found between experiments, simulations and theory.

I. INTRODUCTION

Granular materials come in all shapes and sizes. Idealized spherical particles, have been typically used to unravel the fascinating properties displayed by granular materials. In vibrated granular systems, periodic pattern formation, cluster formation, and complex size separation have been observed. However, anisotropic grains are nearly as numerous, and experience with thermal systems teaches us that shape matters. Only a handful of investigations have studied the impact of anisotropy on granular systems, but the ones that have been accomplished point to a rich phenomenology.

For example, theoretical and numerical study of a low-density gas of hard inelastic needles [1] shows two distinct regimes of cooling related to the different scaling of rotational and translational energy dissipation. In compaction experiments with granular rods [2] granular rods vibrated in a tall narrow container were observed to form ordered stacks i.e. a smectic phase similar to that found in thermal systems, with the additional novelty that the rods align with the gravitation field. More recently, self-organization of vortices was observed to occur when a shallow bed of granular rods was vibrated [3]. It was further shown, that the tilt of the rod and vertical vibration was important to the occurrence of the novel dynamics. While a phenomenological model of formation and growth of the vortices has been proposed [4], a detailed understanding of why the rods move horizontally on a vertically vibrated plate was not reached.

The collective motion of vibrated anisotropic grains is of considerable interest as an example of spontaneous ratchet formation in a non-equilibrium dissipative system. Transport of thermal particles in systems with microscopically asymmetric potential has been studied in a number of recent publications [5]. In Ref. [6], ratchet transport was demonstrated for spherical grains on a vertically vibrated asymmetric saw-tooth profile. In Ref. [7], the transport of elongated grains on a vertically vibrated ratchet-shaped plate has been studied numerically. However, as follows from results of [3, 4], and further described in this paper, the transport of anisotropic grains may occur even without externally imposed microscopic asymmetry of forcing, in which case the direction of motion is chosen as a result of spontaneous symmetry breaking.

In this paper, we apply experimental and numerical tools to a system of rods in a vibrated annular container to elucidate the development of coherent horizontal dynamics in anisotropic systems. This geometry was specifically chosen to simplify the phenomenology in order to focus on the mechanisms for the observed dynamics. Our theoretical model is developed for even simpler quasi-two-dimensional geometry where all rods are confined to a vertical plane, and periodic boundary conditions are imposed. The theory is based on a detailed description of frictional collisions between rods and the vibrating plate which makes use of the assumption of constant kinematic restitution coefficient. While the issues of restitution coefficient in application to frictional impact of asymmetric bodies are still debated in the literature (see, for example, [8]), we show that even this simplest model agrees very well with soft particle molecular dynamics simulations of individual collisions. To describe the collective motion of the rods, we take advantage of the observation that in the regime of stationary translation the mean horizontal mo-

mentum transfer due to the collision with bottom plate is zero, and assume that this condition holds for a typical collision. Our simulations show that during the flight the angular momentum of a single rod is transfered to other rods, so the angular velocity of the rod at the end of the flight becomes small and can be neglected. Furthermore, based on our numerical simulations we make the assumption that the vertical velocity of the center of mass (CM) just before the collision is equal to the CM velocity in the beginning of the flight. These assumptions allow us to find the mean translation CM velocity in a closed form. We show that this theory captures the essential mechanisms of the transport of tilted rods on a vibrating plate.

The paper is organized as follows. First, we introduce the experimental system and report the observed dynamics as a function of the control parameters such as plate acceleration and tilt of rods. Next we discuss the molecular dynamics simulations corresponding to experimental parameters and compare the results with the experimental data. Then using the data as a guide, we construct a theoretical model for the occurrence of spontaneous horizontal motion, and its dependence on control parameters, and compare the results with the data. Finally, we discuss the general implications of this study.

II. EXPERIMENTS

The experimental system consists of an annular container with an inner diameter of 7.28 cm and outer diameter of 9.45 cm, and is similar to that used in Ref. [3]. An image is shown in Fig. 1(a). The sides are composed of clear acrylic and the base plate is made of Aluminum. The container is attached to an electromagnetic shaker through a linear bearing which allows only vertical motion. A frequency generator along with a lock-in amplifier is used to excite the system with a fixed frequency and amplitude. The data reported here for frequency $f = 60$ Hz, and we note that qualitatively similar behavior is observed when the frequency is varied between 50 and 100 Hz. The acceleration of the container is measured with an accelerometer and is reported in terms of Γ, the measured peak acceleration divided by the acceleration due to gravity. The tilt to the rods is characterized by the angle ϕ with respect to the vertical axis.

The rods used for the experiments are cylindrical with a diameter of 0.635 cm and length 5.08 cm. One of the ends is semi-spherical with the radius equal to the radius of the rod, and the other end is flat. The rods are made of a Delrin and Teflon composite, and the measured dissipation coefficients are as follows. The coefficient of static and kinetic friction between the rod and the base plate is 0.36 and 0.25 respectively. The coefficient of restitution is obtained by measuring the kinetic energy of the rod just before and after a collision with a stationary base plate. For nearly normal incidence ($\phi < 5^0$), the coefficient of restitution is approximately 0.8 ± 0.1 (see also [9].) When a single rod is placed inside the annulus, the maximum tilt angle that it can have is 53^0 due the curvature of the annulus. By increasing the total number of rods N in the annulus from $N = 23$ to 56, the tilt ϕ can be varied from 53^0 to 0^0.

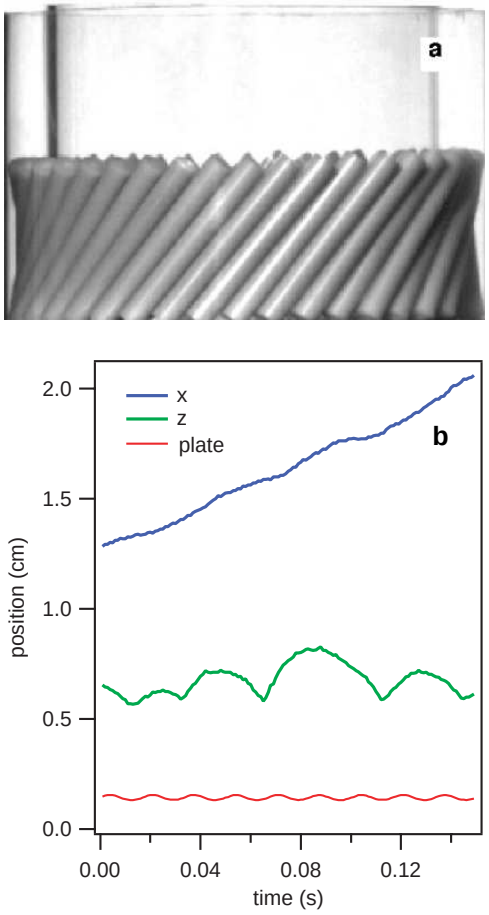


FIG. 1: (a) Annular geometry used in the experiments. (b) The horizontal and vertical position of the rod end at the bottom as a function of time. The position of the oscillating bottom plate is also plotted for reference. The three plots are shifted for clarity. ($\Gamma = 3.3$, $N = 50$, $\phi = 13^0$)

Figure 1(b) shows the typical motion of the bottom tip of a rod as a function of time. The data is obtained by using a high-speed Kodak digital camera with a frame rate of 1000 per second, and tracking the end of the rod with appropriate use of lighting through the transparent side walls. The vertical position of the tip z is observed to oscillate, as the rod bounces on the vibrating plate [also shown in the Fig. 1(b)]. The flight time is observed to vary and although the rod appears to almost always hit the plate on its upstroke, a distribution of phases is observed. We will discuss this issue further after introducing the molecular dynamics simulations in a later section. On the other hand, the horizontal position of the tip is observed to increase approximately linearly although

some oscillatory motion is also seen be superposed. The slope of the x-position gives the average horizontal velocity which is consistent with dividing the average circumference of the annulus by the amount of time taken by the rods to go around once. This second method is used to report observed average horizontal velocities.

The measured horizontal speed c_x as a function of the tilt of the rods ϕ for a fixed $\Gamma = 3.3$ is shown in Fig. 2(a). c_x is observed to increase from zero to a peak value and then decrease. The rods are observed to always move in the same horizontal direction as the tilt. It is to be noted that the error in determining c_x arises from run to run variability due to slight differences in packing inside the annulus rather than from the actual measurement of the velocity itself. In this case, seven separate realizations were used to arrive at the average value of c_x for a particular number of rods.

By varying Γ for a few values of ϕ, we obtain its impact on observed horizontal velocities [see Fig. 2(b).] Positive horizontal velocity is observed to commence only above a finite $\Gamma \sim 1.6$ is reached. Below $\Gamma \sim 1.6$, no net horizontal velocity occurs except for a narrow parameter range where a horizontal motion in a direction opposite to the tilt is observed. As shown in the inset to Fig. 2(c), this reverse horizontal motion is observed to be two orders of magnitude slower than the forward motion.

A phase diagram of the various kinds of observed motion is shown in Fig. 2(d) as a function of Γ and ϕ. Forward motion indicates parameters for which horizontal motion occurs in the direction of tilt, and reverse motion, indicates when the motion is in the opposite direction. The reverse motion is observed to occur only for a narrow range of parameters. The horizontal motion is predominately along the direction of tilt provided a minimum acceleration for the container is achieved.

To study the impact of the shape of the rod tip, we also performed experiments by flipping the rods so that the flat end is at the bottom. Figure 2(c) compares the measured c_x as a function of Γ for rods with rounded and flat ends but otherwise under identical conditions. When the flat end interacts with the bottom plate, the observed horizontal velocities are lower, the minimum rod tilt required to obtain horizontal motion is 8^0, but otherwise the qualitative phenomena remains the same.

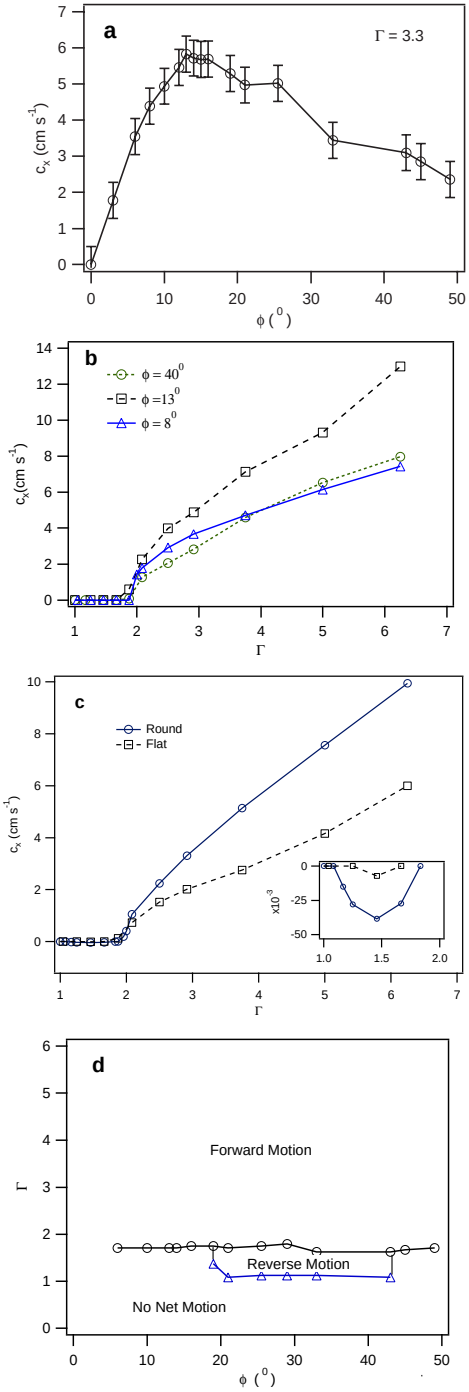


FIG. 2: (a) The average horizontal velocity c_x of the rods as a function of tilt angle ϕ. (b) c_x versus Γ for three different tilt angles. (c) The effect of rod end shape on measured c_x. A flat end rod is observed to move slowly compared to a rod with a round end. Horizontal motion in a direction opposite to the tilt is observed over a small range of low Γ. ($\phi = 28^0 \pm 2^0$) Inset: c_x measured between $\Gamma = 1$ and 2 is replotted to clarify the small magnitude of the reverse motion. (d) A phase diagram denoting the kinds of horizontal velocity observed relative to the direction of the tilt. The rods are observed to move in the direction of the tilt under most conditions.

III. NUMERICAL SIMULATIONS

We performed a series of numerical simulations of the bouncing rods on a vibrated plate. The rods are modeled as spherocylinders of diameter d, length l, mass m, and moment of inertia I. A rod has three translational and two rotational degrees of freedom, the rotation of a rod around its own axis is neglected. Our numerical algorithm is based on the "soft spheres" molecular dynamics technique [10]. The interaction forces between colliding spherocylinders are calculated via the interaction between viscoelastic virtual spheres of diameter d

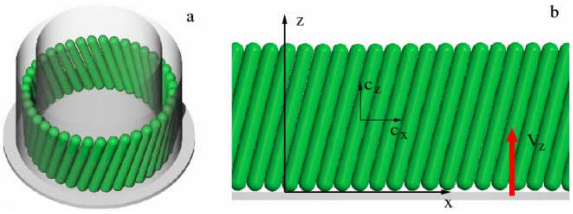


FIG. 3: Two types of geometry used in simulations: (a) - annulus geometry, (b) - quasi-2D geometry with periodic boundary conditions along x where the motion of rods is constrained to the $x-z$ plane.

centered at the closest points between the axes of spherocylinders, so that the cylinders are in contact whenever virtual spheres are. The normal forces between virtual spheres are computed using Hertzian model and the tangential frictional forces are computed by the Cundall-Struck algorithm. They lead to the kinematic restitution coefficient of about 0.65-0.7 slightly varying with impact angle. In most cases we used equal friction coefficients $\mu_{rr} = \mu_{rb} = \mu_{rw} = 0.3$ for all sliding surfaces (rod-rod, rod-bottom and rod-side wall) and ignored the difference between dynamic and static friction coefficients while comparing to experiments. The forces arising from the interaction of virtual spheres are then applied to the rods (see Appendix A for details). The motion of rods was obtained by integrating the Newton's equations with the forces and torques produced by interactions of a rod with all the neighboring rods, walls of the container, and by gravity.

Figure 3 illustrates two configurations employed in numerical simulations. An annular geometry [Fig. 3(a)] was used to match closely the experimental setup. However, to separate the effects of side wall friction and oblique collisions among the rods due to annulus curvature, we also studied the quasi-2D geometry of Fig. 3(b) in which axes of all rods are constrained to the $x-z$ plane. This geometry is more amenable to the theoretical analysis and was used for comparison with our theoretical predictions.

In simulations we observed robust drift of the rods in the direction of inclination in agreement with experiments [13]. Figure 4(a) shows the translation velocity as a function of the inclination angle for the annulus geometry and parameters $f = 60$ Hz and $\Gamma = 3.3$ used in experiments. The translation velocity grows linearly for small ϕ, reaches maximum at $\phi \approx 18^o$ and also for $\phi \approx 35^o$ after which it decays to zero at large ϕ. For intermediate inclinations, $18^o < \phi < 35^o$, in most cases we observed noticeable slowdown which however is not typically observed in experiment. We will discuss the source of this discrepancy below.

Figure 4(b) shows the dependence of the average translational velocity of rods on the acceleration of the container at fixed frequency for a number of inclinations. As in experiments the motion starts above a (slightly lower)

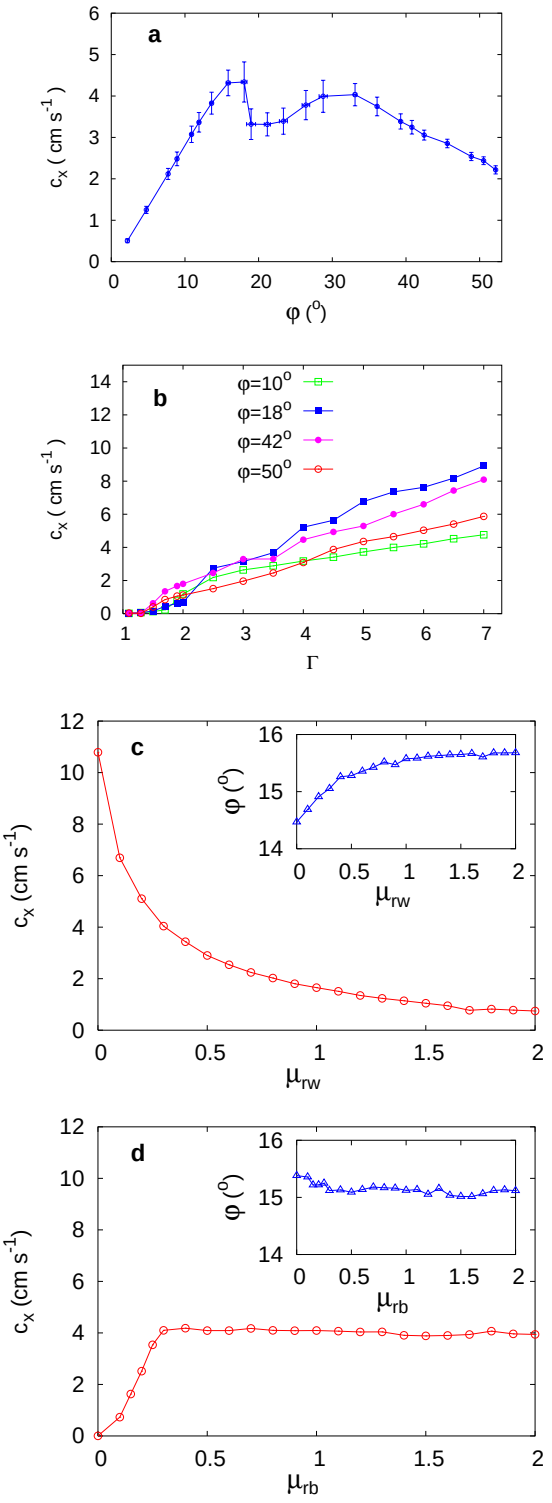


FIG. 4: The results of simulations in the annular geometry: (a) - average translational velocity of rods as a function of tilt at $f = 60Hz$,$\Gamma = 3.3$; (b) - *idem* as a function of Γ for a number of tilt angles; (c) - *idem* and average tilt as a function of the coefficient of friction between the rods and the walls; (d) - *idem* and average tilt as a function of the coefficient of friction between the rods and the bottom.

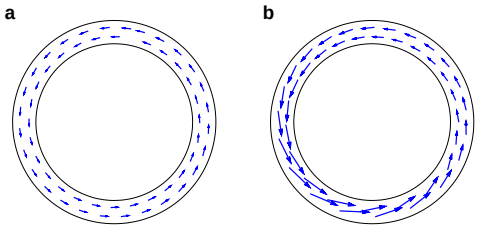


FIG. 5: The results of simulations in the annular geometry illustrating formation of the non-uniformity in the tilt for $f = 60Hz$, $\Gamma = 3.3$. Shown are (normalized) horizontal projections of the rods' directors for two numbers of rods (a) $N = 55$, (b) $N = 44$, the mean tilts are $\phi \approx 9^o$ and $\phi \approx 22^o$ respectively.

threshold $\Gamma > 1.5$. Above $\Gamma \approx 2.0$ this velocity grows roughly linearly with the acceleration. We explain the presence of the threshold by the friction with side walls. Indeed, in the experiments in quasi-2D geometry there is no threshold and $c_x \propto \Gamma - 1$ right down to $\Gamma = 1.0$. Figure 4(c) depicts explicitly how the average translational velocity and average tilt depend on the coefficient of friction with the sidewall μ_{rw}, for a fixed number of rods. As one could expect this dependence shows monotonic decay when μ_{rw} is increased; less expected is more than ten-fold difference in velocities for large and small μ_{rw} which probably explains systematically slower translational velocities in simulations and underlines an importance of the proper account of friction with walls.

Next, to eliminate the effects of the curved side walls and out-of-plane rod-rod collisions, we simulated the collective rod motion in a quasi-2D geometry with periodic boundary conditions along the direction of the rod tilt [Figure 3(b)]. All rods are confined strictly to the $x - z$ plane, and the interaction with side walls was ignored, while friction with the vibrating bottom plate and among the rods was taken into account. We used a fixed number of rods ($N = 40$) and varied the length of the container, thereby changing the tilt angle ϕ [see Figure 3(c)]. The relation between the length and the tilt is well described by a simple formula $\cos\phi = dN/L$.

Figure 6(a-c) the mean values of rod velocities before and after impacts. As seen from Fig. 6(a), the angular velocity before the collision is rather small (apparently, it decays after inelastic collisions with other rods during flight). Figures 6(b,c) shows the horizontal and vertical CM velocities of rods just before and after collision in the laboratory frame as a function of ϕ. As seen from these plots, the pre- and post-collisional velocities are close to each other. The mean velocity of the plate at the moment of collision is shown in Fig. 6(d). The velocity is only weakly dependent on ϕ and is close to $V_0/2$. In Fig. 6(a) one can also see a noticeable variation of the horizontal translation velocity near $\phi = 30^o$ which however is not accompanied by a sharp drop at $\phi \approx 20^o$ observed in 3D geometry.

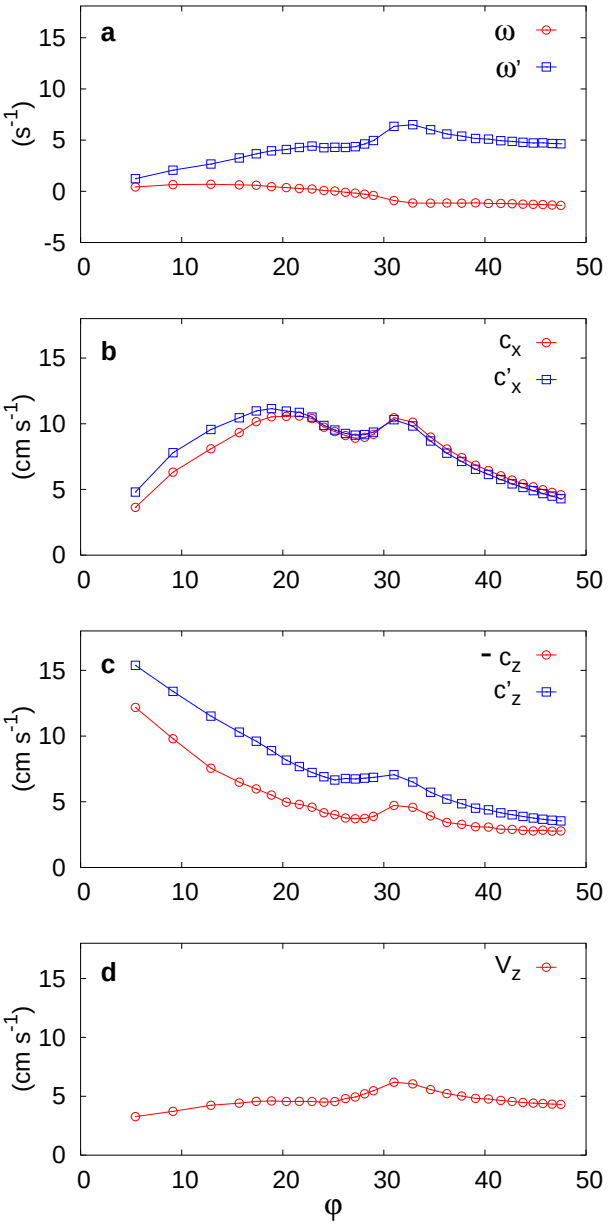


FIG. 6: The mean CM velocities of rods before (black) and after (red) collision as a function of inclination angle ϕ in quasi-2D numerical simulations. The parameters are $l = 9.5d$, $\Gamma = 3.3$, $\mu = 0.3$. For comparison with experiments the velocities are plotted in dimensional units for experimental values of $d = 0.6cm$ and $f = 60Hz$: (a) angular velocities ω and ω'; (b) vertical CM velocities $-c_z$ and c'_z; (c) horizontal CM velocities c_x and c'_x; (d) the mean plate velocity at the time of collision.

We conclude that there are two different mechanisms which independently contribute to the slowdown of rods at intermediate values of tilt angle. The first mechanism that only operates in 3D geometry is related to the

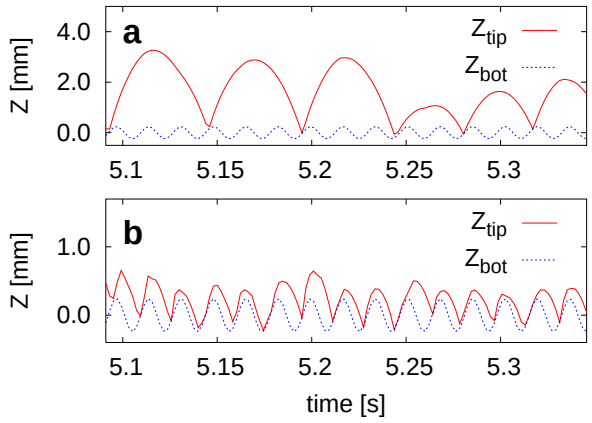


FIG. 7: Typical trajectories of the tip of a rod in numerical simulations for two different tilt angles $\phi = 9^o$ and 34^o (other parameters are the same as in Fig. 6

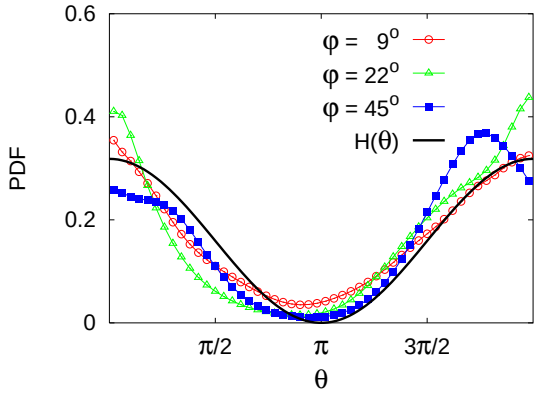


FIG. 8: Distribution of collision times of rods over the phases of the plate vibration for different values of the tilt angle ϕ. Solid line: approximation $H(\theta) = (1 + \cos\theta)/2\pi$ used for the theoretical analysis, where θ is the phase of the plate velocity, $V_{pl} = V_0 \cos\theta$. Parameters are the same as in Fig. 6.

spontaneous formation of the non-uniformity of rod arrangement in an annulus at intermediate inclination angles. For small tilt, the rods are arranged in a uniform hexagonal-like packing (see Fig. 5) with one rod near the inner wall of the gap, next near the outer wall and so on. This "perfect" arrangement may be perturbed by the presence of one or few one-rod defects due to geometrical frustration, however their cumulative effect is quite small and does not change the collective motion considerably. At $\phi \approx 18^o$ in most of the numerical experiments, the hexagonal packing spontaneously breaks and as a result a localized region with much larger tilt emerges. At $\phi \approx 25^o$ it involves roughly half of the rods [Fig. 4(e)]. Eventually, this region spans the whole perimeter and the dependence $c_x(\phi)$ becomes smooth again. This defect appears to play a significant role in slowing down the rods drift. This effect is exacerbated in numerical simulations by neglecting the rod rotation around its axis. Therefore, rolling of rods along the side walls is prohibited by the numerical model, and thus the sidewall friction is effectively enhanced.

The second mechanism operates both in 2D and 3D, and it has to do with the bifurcation between long flights spanning more than one period of vibrations at small tilt angles and short flights which last one period of vibration at large tilt angles (see Figure 7). This transition occurs at $\phi \approx 30^o$ and it leads to the noticeable difference in the distribution of the landing times over the phase of the plate vibrations for different tilt angles (see Figure 8). At large angles the landing times are mostly confined to the phase interval in which the plate moves upward, whereas at smaller tilt angles there is a significant probability of collisions during the downward motion of the plate ($\pi/2 < \theta < 3\pi/2$), where $\theta = \mathrm{mod}(2\pi f t, 2\pi)$. This bifurcation explains the bump in the dependence of the mean vertical plate velocity at impact [see Fig. 6(d)] and correspondingly the horizontal translation velocities c_x, c_x' on the tilt angle [see Fig. 6(b)].

Overall, our simulations show that the side walls do play an important role in determining the magnitude of the horizontal velocity of rods. As seen from comparison of Figs. 4 and 13, the transport velocity in quasi-2D case is 2.5 times greater than in the annulus for the same values of parameters. On the other hand, they allow us to develop a theoretical model of the collective rod motion based on the observations that, to a first approximation, the pre- and post-collision center of mass translation speeds are close to each other and that the angular velocity before the collision can be neglected.

IV. ROD COLLISION WITH PLATE

In this section we derive the necessary formulas for an isolated collision between a rod and a vertically moving plate. We confine the analysis to the case of in-plane, eccentric, oblique frictional impact. Our derivation is based on the classical analysis which assumes the constant kinematic restitution coefficient (see Ref. [8]).

Consider uniform rigid rod of mass m and length l colliding with a plate at point O (see Fig 9). We place the system of coordinates at point O so that the common normal $\mathbf{n}$ coincides with the ort $\hat{\mathbf{z}}$ and the axis of rod, prescribed by unit vector $\mathbf{u}$, is in the $x - z$ plane, $\mathbf{u} = (\sin(\phi), 0, \cos(\phi))$. Prior to the collision, the rod has translational velocity (associated with the center of mass G) $\mathbf{c} = (c_x, 0, c_z)$, and angular velocity $\omega = (0, \omega_y, 0)$, and the plate has only vertical velocity $\mathbf{V} = (0, 0, V_z)$. The corresponding post-collisional velocities of rod are denoted by primes.

Newton's second law gives equations for translational and rotational motion of the rod. In differential form

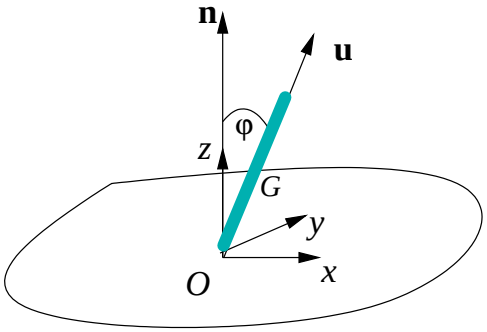


FIG. 9: Geometry of the collision between rod and sphere.

they read,

$$m d\mathbf{c} = d\mathbf{P}, \tag{1}$$

$$I d\omega = -\frac{l}{2}\mathbf{u} \times d\mathbf{P} \tag{2}$$

where I is the moment of inertia of a rod for its rotational motion around the center of mass G. $d\mathbf{P} = \mathbf{F}dt$ is the differential of the impulse $\mathbf{P}$ exerted on the rod during the collision.

The impulse acquired by the rod is the integral of the reaction force over the time of collision. The reaction force depends on the relative velocity at the contact point (CP),

$$\mathbf{v} = \mathbf{c} - \frac{l}{2}\omega \times \mathbf{u} - \mathbf{V}. \tag{3}$$

The Newton's law for the velocity of the contact point (CP) reads

$$m\frac{d\mathbf{v}}{dt} = \mathbf{F} + \alpha[\mathbf{F} - \mathbf{u}(\mathbf{F}\cdot\mathbf{u})] \tag{4}$$

or, in projections,

$$m\dot{v_x} = -\frac{XZ}{k^2}F_z + \frac{k^2+Z^2}{k^2}F_x \tag{5}$$

$$m\dot{v_z} = \frac{k^2+X^2}{k^2}F_z - \frac{XZ}{k^2}F_x \tag{6}$$

where X, Z are coordinates of the center of mass (CM) of the rod, and k is the radius of gyration of the rod. In writing (4) we assumed that the time of collision is so short that we can neglect the changes in the plate position and velocity. Depending on initial conditions, the impact proceeds according to one of three different scenarios.

Slide. Let us denote the duration of the contact t_f, so $F_z(0 < t < t_f) > 0, F_z(0) = F_z(t_f) = 0$. We assume that at $t = 0$, $v_x(0) = u_0 > 0$ and $v_z(0) = v_0 < 0$. After initial contact, the rod slides along the plate, so $F_x = -\mu F_z$ (for brevity we dropped the subscript rb of the friction coefficient). If

$$u_* \equiv u_0 - \frac{XZ + \mu(k^2+Z^2)}{mk^2}P_z(t_f) > 0 \tag{7}$$

[here $P_z(t) = \int_0^t F_z(t)dt$] the slip in positive direction continues throughout the contact, and $u_f \equiv u(t_f) = u_*$. While the total impulse $P_z(t_f)$ is not known a priori, it can be determined from the kinematic condition $v_f = -\epsilon v_0$ assuming that (7) is satisfied. Then integrating Eq.(6) from $t = 0$ to t_f we get

$$P_z(t_f) = -v_0(1+\epsilon)\frac{mk^2}{k^2+X^2+\mu XZ} \tag{8}$$

and correspondingly

$$P_x(t_f) = v_0(1+\epsilon)\frac{m\mu k^2}{k^2+X^2+\mu XZ}. \tag{9}$$

Now we can calculate the CM velocities after the contact using

$$c'_x = c_x + P_x(t_f)/m, \tag{10}$$

$$c'_z = c_z + P_z(t_f)/m. \tag{11}$$

Replacing $u_0 = c_x - \omega Z$ and $v_0 = c_z - V_z + \omega X$ we get the center of mass (CM) velocities immediately after the collision

$$c'_x = c_x + \frac{\mu(1+\epsilon)k^2(c_z - V_z + \omega X)}{\mu(k^2+Z^2)+XZ}, \tag{12}$$

$$c'_z = cz - \frac{(c_z + \omega_x - V_z)(1+\epsilon)k^2}{\mu(k^2+Z^2)+XZ} \tag{13}$$

Using (8) the no-stop sliding condition (7) can be written as

$$u_* \equiv u_0 + \frac{XZ + \mu(k^2+Z^2)}{k^2+X^2+\mu XZ}v_0(1+\epsilon) > 0 \tag{14}$$

If the condition (14) is violated, at a certain time t_1 during collision the sliding stops, $v_x(t_1) = 0$. At $t = t_1$, the horizontal CP velocity $u_1 = 0$ and the vertical CP velocity is

$$v_1 = v_0 + \frac{k^2+X^2+\mu XZ}{\mu(k^2+Z^2)+XZ}u_0. \tag{15}$$

At $t > t_1$ the contact may remain at rest or reverse the direction of sliding.

Slip-stick. If

$$\mu(k^2+Z^2) > XZ, \tag{16}$$

the contact sticks, and the horizontal velocity $u(t_1 < t < t_f) = 0$. During this phase,

$$F_x = \frac{XZ}{k^2+Z^2}F_z \tag{17}$$

Assuming again the kinematic restitution law $v_f = -\epsilon v_0$, we derive the expression for the CM velocity at the end of the collision (see Appendix B):

$$c'_x = \frac{(c_x - \omega Z)Z^2 - (c_z - V_z + \omega X)(1+\epsilon)XZ}{k^2 + X^2 + Z^2} + \omega Z \quad (18)$$

$$c'_z = \frac{(c_z - V_z + \omega X)[X^2 - (k^2 + Z^2)\epsilon] - (c_x - \omega Z)XZ}{k^2 + X^2 + Z^2} + V_z - \omega X \quad (19)$$

Note that for the case of slip-stick, the post-collisional velocities are independent of the friction coefficient.

Slip reversal. If

$$\mu(k^2 + Z^2) < XZ, \quad (20)$$

the contact slides back after stopping. In this phase $F_x = \mu F_z$. Again omitting the details of derivation (see Appendix B) we give here the formulas for the CM velocity at the end of collision:

$$c'_x = c_x + (c_x - \omega Z)\frac{2\mu k^2(k^2 + X^2)}{(\mu(k^2 + Z^2) + XZ)(k^2 + X^2 - \mu XZ)} - (c_z - V_z + \omega X)\frac{\mu k^2(1+\epsilon)}{k^2 + X^2 - \mu XZ} \quad (21)$$

$$c'_z = c_z - (c_x - \omega Z)\frac{2\mu k^2 XZ}{(\mu(k^2 + Z^2) + XZ)(k^2 + X^2 - \mu XZ)} - (c_z - V_z + \omega X)\frac{k^2(1+\epsilon)}{k^2 + X^2 - \mu XZ} \quad (22)$$

Thin rod. For a thin rod of length l, we use values $X = l\sin\phi/2, Z = l\cos\phi/2, k = l/2\sqrt{3}, I = ml^2/12$. Let us first outline the boundaries of three different regimes (continuous slide, slip=stick, and slip reversal) in the (ϕ, μ) parameter plane. While the condition for the transition from slip-stick to slip reversal is universal, the condition of continuous slide (14) depends on the values of ϵ and the ratio c_z/c_x and ω. Figure 10 shows the bifurcation diagram for $\epsilon = 0.8$ and three different values of $-c_z/c_x$ for $\omega = 0$. Typically this ratio is large, so the regime of sliding can only be observed for small $\mu < \mu_c = -c_x[4c_z(1+\epsilon)]^{-1}$ and either large or small ϕ. For larger $\mu > \mu_c$, at small ϕ the slip-stick regime occurs, and at larger angles there is the slip reversal regime. The critical angle ϕ_c at which the transition from slip-stick to slip reversal occurs, is determined from equation for ϕ_c $(3\sin\phi_c\cos\phi_c = \mu(1 + 3\cos\phi_c^2)$. Solving this equation, we obtain

$$\phi_c = \frac{1}{2}\arccos\frac{\sqrt{9 - 16\mu^2} - 5\mu^2}{3(1+\mu^2)} \quad (23)$$

For small μ, $\phi_c = \frac{4}{3}\mu + O(\mu^3)$. Note that the critical angle is only dependent on the friction coefficient μ and becomes $\pi/2$ at $\mu = 3/5$. At larger μ, the slip-reversal scenario does not occur at any tilt angle.

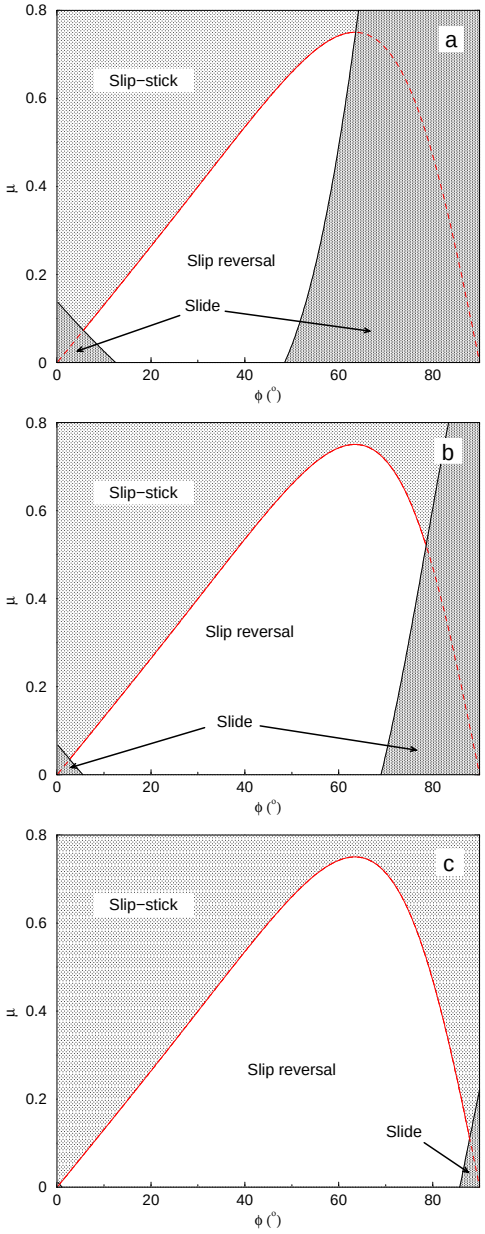


FIG. 10: Bifurcation diagrams of single rod collision with a plate for $\epsilon = 0.8$ and three different values of $-c_z/c_x$: 1 (a), 2 (b), and 10 (c).

V. COLLECTIVE MOTION OF RODS

In order to analyze the collective motion of bouncing rods using the results for an individual rod collision obtained in the previous section, we have to make additional assumptions regarding the interactions of rods. In the formulation of these assumptions, we use the numerical and experimental observations. Referring to Figure 6(a-c), we assume that in the stationary translation regime, $\omega = 0, c_x = c'_x, c_z = -c'_z$. Note that the latter simple assumption is not very accurate for large Γ and small ϕ,

however using it still leads to a reasonable agreement between the theory and simulations. A more accurate set of closure conditions would require a detailed description of the complicated interactions of the rod during the flight between two consecutive collisions.

Adopting these simplifications, we immediately arrive to the relations for the horizontal and vertical velocities of the rods. Note that among the three cases outlined above, the sliding regime cannot be realized in the regime of stationary translation, since it would imply a continuous decay of c_x. So eventually one of the two other regimes will be established depending on the inclination angle (in a finite container, the dynamically selected inclination angle is weakly dependent on the driving acceleration, see inset in Fig. 13(b)).

Slip-stick. Assuming $c_x' = c_x$, $c_z' = -c_z$, and $\omega = 0$, we get from (18), (19) in the slip-stick regime ($\phi < \phi_c$)

$$c_x' = \frac{2(1+\epsilon)XZV_z}{k^2(1-\epsilon)+2X^2} \quad (24)$$

$$c_z' = \frac{(1+\epsilon)k^2V_z}{k^2(1-\epsilon)+2X^2} \quad (25)$$

For a thin rod, Eq.(24) yields

$$c_x' = \frac{6(1+\epsilon)\sin\phi\cos\phi}{1-\epsilon+6\sin^2\phi}V_z \quad (26)$$

Slip reversal. In the slip-reversal regime ($\phi > \phi_c$), we solve Eqs.(21),(22) with constraints $c_x = c_x'$, $c_z = -c_z'$, $\omega = 0$. As a result, we get

$$c_x' = \frac{(1+\epsilon)\mu(k^2+Z^2)V_z + (1+\epsilon)XZV_z}{k^2(1-\epsilon)+2X^2} \quad (27)$$

$$c_z' = \frac{(1+\epsilon)k^2V_z}{k^2(1-\epsilon)+2X^2} \quad (28)$$

Note that the vertical velocity c_z' is again independent of μ and in fact coincides with (25). It is easy to see that in the transition point from slip-stick to slip reversal regime where $XZ = \mu(k^2+Z^2)$ the values of the horizontal translation speed (24) and (27) coincide.

For a thin rod case, we obtain from Eq.(27)

$$c_x' = \frac{(1+\epsilon)[\mu(1+3\cos^2\phi)+3\sin\phi\cos\phi]}{1-\epsilon+6\sin^2\phi}V_z \quad (29)$$

The vertical velocity after collision is given by

$$c_z' = \frac{1+\epsilon}{1-\epsilon+6\sin^2\phi}V_z \quad (30)$$

in both slip-stick and slip reversal regimes. Figure 11 shows the dependence of the normalized vertical velocity and the translation speed $c_z'/V_z, c_x'/V_z$ on the inclination angle ϕ for the case $\omega = 0$. The transition from slip-stick to slip reversal dependence occurs at ϕ_c.

The remaining question is what is V_z? Obviously V_z is smaller than the amplitude V_0 of the plate velocity

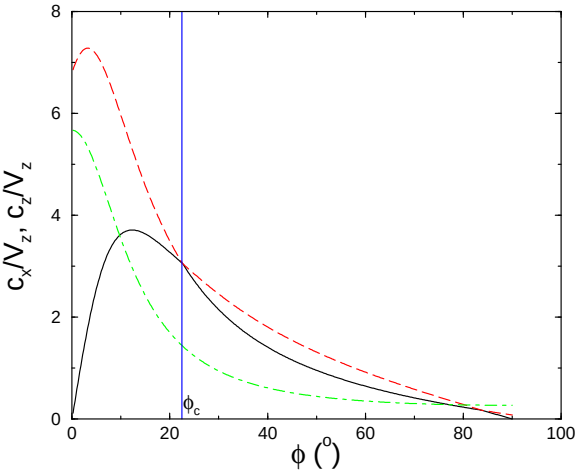


FIG. 11: Normalized vertical velocity after collision c_z'/V_z (green dot dashed line) and the translation velocity c_x'/V_z (black solid line) as a function of the inclination angle for $\epsilon = 0.65, \mu = 0.3$. Red dashed shows the unphysical branches of the slip-stick and slip reversal dependencies (18), (21) for the horizontal post-collisional velocity.

$V = V_0\cos(\Omega t)$, because the rods collide with the plate at different phases and not only at phase 0 when $V = V_0$. A simple assumption which we are going to make is that $V_z = \alpha V_0$ with a constant fitting parameter $\alpha < 1$. In fact our numerical simulations indicate that α is close to 0.5 but varies slightly with ϕ because the landing phase distribution depends on ϕ (see Figure 8), but for the sake of simplicity we shall ignore this dependence. The value $\alpha = 0.5$ is obtained if we approximate the distribution of collision phases as $H(\theta) = (1+\cos\theta)/2\pi$, where θ is the phase of the plate velocity, $V_{pl} = V_0\cos\theta$. Then we obtain for the average plate speed at collision,

$$V_z = V_0(2\pi)^{-1}\int_0^{2\pi}\cos\theta(1+\cos\theta)d\theta = V_0/2 \quad (31)$$

At small $0 < \Gamma - 1 < 1$, the distribution deviates significantly from $H(\theta)$. The rods only leave the plate for short flights near the top position of the plate at which the vertical acceleration is smaller than $-g$, and the vertical velocity V is close to zero. Due to inelasticity, after landing the rod may perform a few more smaller bounces before coming to rest until the next period. While it is difficult to describe this regime analytically, one can expect that $V_z \propto \Gamma - 1$ at small Γ.

VI. DISCUSSION

In this section we compare the theoretical results with numerical simulations for the quasi-2D case. First, we tested the theoretical predictions for the isolated rod bounced off the plate, and found a good agreement between formulas (12), (13), (18), (19), (21), (22), and

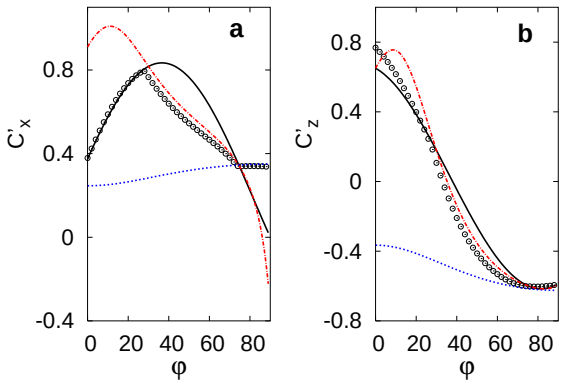


FIG. 12: Post-collisional CM velocities c'_x and c'_z as a function of tilt angle for $\mu = 0.4$ and $-c_z/c_x = 2$. Symbols indicate the results of numerical simulations, and lines show theoretical predictions for different collision scenarios using constant coefficient of restitution, $\epsilon = 0.65$. Solid lines denote slip-stick, dash lines denote continuous slip, and dash-dot lines denote slip-reversal.

numerics (see Fig. 12). One can clearly see the transitions between three different regimes of rods bouncing: slide, slip-stick, and slip reversal. A slight difference between the theory and simulations in the vertical velocity at small tilt angles is related to the above-mentioned variations of the kinematic restitution coefficient with tilt angle in soft-particle MD simulations which was ignored in an analytical calculations.

A comparison between the theory and MD simulations for the mean translation velocity is shown in Figure 13. Figure 13(a) shows the horizontal translation velocity as a function of the mean tilt angle. The overall dependence is in reasonable agreement with the theory, however some noticeable differences are obvious. This should not be surprising, given the crude assumptions made to describe the dynamics of rods during flights between collisions. As mentioned above, the 'bump' visible at $\phi \approx 30^o$ is related to a transition from the regime of 'long' flights that span more than one period of vibrations, to the 'short' flights that last a fraction of the period of vibrations. As seen in Figure 8, these two regimes are characterized by significantly different distributions of the collision times over the vibration phases.

Figure 13(b) shows the Γ dependence of the horizontal translation velocity. As expected from the theory, and seen in experiments, the horizontal translation velocity is linearly proportional to Γ at large Γ. Unlike the annular case, the translation velocity turns zero at $\Gamma = 1$, and indeed it grows as $\Gamma - 1$ at small $\Gamma - 1$. Figure 13(c) addresses the question of the rod length dependence of the horizontal translation velocity. According to the theory for thin rods, c_x should be independent of l. On the other hand, the drift should disappear when the aspect ratio of the rod approaches 1 (the case of spherical particles). As seen in Figure 13(c), the translation velocity grows linearly at small $l > 1$, but this growth saturates at $l \approx 3$ after which the translation velocity is independent of l in agreement with the theory.

There are several possible sources of discrepancies between the theory and numerics (and experiments). First, in describing individual collisions we made an implicit assumption that the collision time is small as compared with the period of oscillations. This assumption may break for high frequency vibrations or in the regime of small Γ when rods spend a significant portion of the period in contact with the plate. Furthermore, we used the simplest closure assumptions to relate the horizontal and vertical velocities of rods after and before the flight. While the relation $c_x = c'_x$ appears to work well throughout the range of parameters corresponding to experimental conditions, the other condition $c_z = -c'_z$ holds only approximately. Our numerical experiments showed a significant (up to 50%) deviations from this simple relation at large Γ, when many inelastic collisions occur during the flight. We were unable to describe this effect theoretically, and chose to sacrifice the accuracy of comparison rather than introduce an unknown fitting parameter $-c_z/c'_z$.

Comparison between 2D and 3D simulations (Figs. 4, 13) shows that the characteristic translation velocity in 3D case is 2.5 times smaller than in 2D case with the same material parameters. This difference may be accounted for by the frictional interaction with side walls. We systematically studied the dependence of the translation velocity in the annulus on the friction coefficient μ_{rw} between the rods and the side walls, and found that indeed it varies strongly with μ_{rw}, in particular, the translation velocity at $\mu_{rw} = 0.3$ is 2.5 times smaller than c_x at $\mu_{rw} = 0$ (see Fig. 13(b)). We also analyzed the dependence of the translation velocity on the friction coefficient with the bottom, and found that for large μ_{rb} the translation velocity becomes independent of μ_{rb}. This is consistent with the theoretical argument that at large μ_{rb} the slip-stick scenario occurs for an arbitrary tilt angle ϕ.

As a conclusion, we studied experimentally and theoretically the drift of anisotropic particles (rods) on a vibrated plate. The experiments in the annulus showed the robust drift of rods in the direction of their tilt, at the normalized vertical acceleration $\Gamma > 1.5$. For smaller values of $1 < \Gamma < 1.5$, very small *reverse* drift was observed. We developed a novel numerical algorithm which allowed us to study the interaction of rods in soft-particle MD simulations. Simulations of rods in an annulus with parameter closely matched experiment, revealed very similar behavior, both qualitatively and quantitatively.

Out theoretical description of the rod translation is based on the detailed analysis of frictional collisions between an individual rod and the moving plate. The effects of collective interaction of rods during flights between collisions are taken into account using the simplest phenomenological closure conditions based on the experimental findings and MD simulations. As a result,

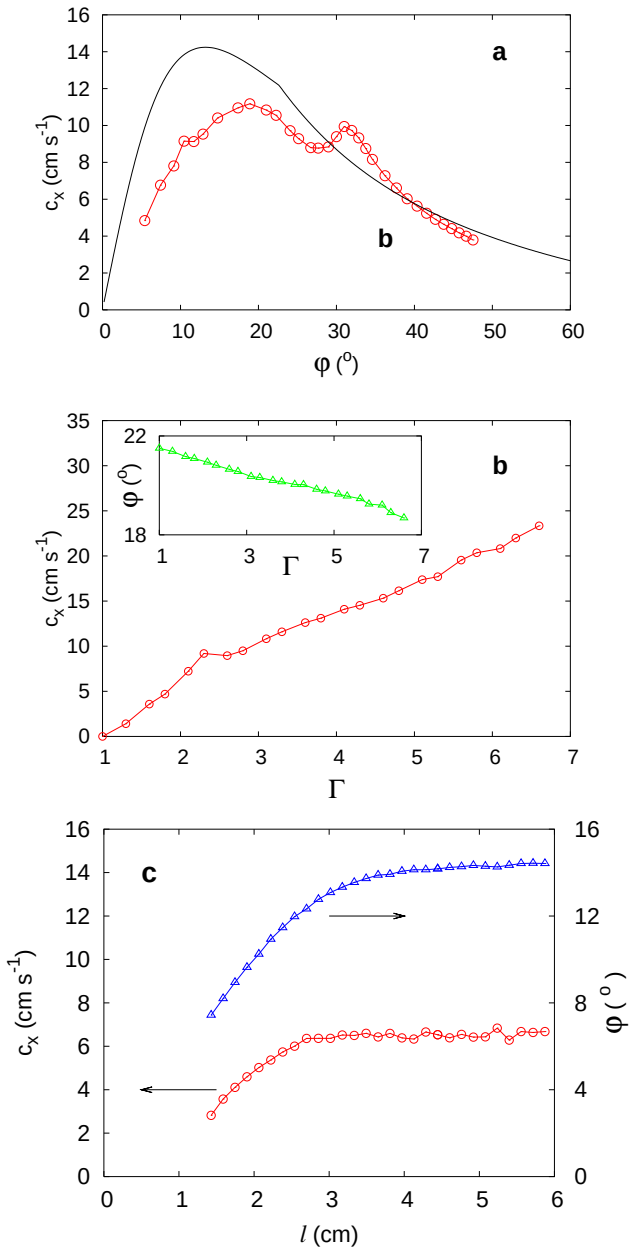


FIG. 13: Results of simulations in quasi-2D geometry. $N = 40$ rods are placed in a periodic domain of different lengths L which determine the tilt angle ϕ_0. (a) - average horizontal velocity of rods as a function of the inclination angle for $\Gamma = 3.3$, solid line - theory (24), (29), (31) with $\epsilon = 0.65, \mu = 0.3$; (b) - average horizontal velocity of rods and average tilt (inset) as a function Γ for $L = 43$; (c) average horizontal velocity of rods and average tilt as a function of the length of rods $l = h_0 + 1$, where h_0 is the distance between the centers of spherical caps. $N = 40$ rods are placed in a periodic domain of length $L = 41.4$ [12], the bottom is oscillating at frequency $f = 60Hz$ and acceleration is $\Gamma = 2.5$.

closed formulas for the horizontal translation velocity are obtained. A direct comparison between the theory and experiments is complicated by the role of interaction of rods with frictional side walls which is unaccounted for in the theory. However, we found a reasonable agreement between the theory and numerics for quasi-2d geometry when rods are confined to the $x - z$ plane with periodic in x boundary conditions. Since the same numerical code describes well the experiment in the annulus geometry, we infer that the theory correctly captures the mechanism of the rod translation in experiment.

Some more subtle effects are, however, are difficult to model theoretically. The (very slow) reverse drift of rods for small Γ is presumably due to the small negative value of average V_z, however to calculate the mean V_z one needs a detailed knowledge of the distribution of landing times for small Γ which is difficult to obtain theoretically.

We thank Daniel Blair for help with performing preliminary experiments and for many helpful discussions. This work was funded by the NSF Grant # DMR-9983659 (AK) and the U.S. Department of Energy, Office of Basic Energy Sciences, under grant # DE-FG03-95ER14516 (DV and LT).

[1] M. Huthmann, T. Aspelmeier, and A. Zippelius, Phys. Rev. E **60**, 654 (1999).

[2] F.X. Villarruel, B.E. Lauderdale, D.M. Mueth, and H.M.

Jaeger, Phys. Rev. E **61**, 6914 (2000).
[3] D.L. Blair, T. Neicu, and A. Kudrolli Phys. Rev. E **67**, 031303 (2003).
[4] I.S. Aranson and L.S. Tsimring. Phys. Rev. E **67**, 021305 (2003).
[5] M. Magnasco, Phys. Rev. Lett. **71**, 1477 (1993); R. D. Astumian and M. Bier, Phys. Rev. Lett. **72**, 1766 (1994); C. R. Doering, W. Horsthemke, and J. Riordan, Phys. Rev. Lett. **72**, 2984 (1994); P. Jung, J. Kissner, and P. Hanggi, Phys. Rev. Lett. **76**, 3436 (1996); I. Derényi and T. Vicsek, Phys. Rev. Lett. **75**, 374 (1995).
[6] Z. Farkas, P. Tegzes, A. Vukics, and T. Vicsek, Phys. Rev. E **60**, 7022 (1999).
[7] J.F. Wambaugh, C. Reichhardt, and C.J. Olson Phys. Rev. E **65**, 031308 (2002).
[8] W.J. Stronge, Proc. Roy. Soc. London A, **431**, 169 (1990); D. Stoianovici and Y. Hurmuzlu, ASME J. Appl. Mech., **63**, 307 (1996).
[9] D.L. Blair, Ph.D. Dissertation, Clark University (2004).
[10] P. A. Cundall and O. D. L. Strack, *Géotechnique* **29,** 47 (1979); J. Schäfer, S. Dippel, and D.E. Wolf, J. Phys. I France **6**, 5 (1996); H.J. Herrmann, S. Luding, Continuum Mech. Therm., **10** (4) 189 (1998); A. Dziugys , B. Peters, Granular Matter, **3** (4), 231(2001); L. E. Silbert, D. Ertas, G. S. Grest, T. C. Halsey, D. Levine, and S. J. Plimpton, Phys. Rev. E **64**, 051302 (2002).
[11] With this approach the steric exclusion is modeled more accurately than in the case when the rod is approximated by a row of fixed spheres. On the other hand the most time-taking operation of soft-spheres MD, finding the overlap, is reduced to minimization of the quadratic form (finding the closest point between two segments).
[12] In contrast with the rest of the paper we assumed that rods are actual spherocylinders with dimensionless mass $1 + 3/2h_0$ and moment of inertia $1/10 + 15/32h_0 + h_0^2 + 1/8h_0^3$
[13] Movies of the rods drift in numerical simulations can be found at http://inls.ucsd.edu/grain/rods.
[14] M. P. Allen and D. J. Tildesley, *Computer Simulations of Liquids* (Oxford University Press, Oxford, 1987).

APPENDIX A: MOLECULAR DYNAMICS ALGORITHM

In our MD algorithm, two virtual spheres of diameter d, with centers at $\mathbf{r}_i$ and $\mathbf{r}_j$, and with velocities $\mathbf{v}_i$ and $\mathbf{v}_j$, interact via normal and tangential forces, $\mathbf{F}_{ij} = F_n\mathbf{n}_{ij} + \mathbf{F}_t$, $F_n = k_n\delta^{3/2} - \gamma_n M_e \delta v_n$. We introduce tangential spring with deflection obtained by the integration of tangential velocity through the period of impact, $\mathbf{s} = \int d\tau \mathbf{v}_t$, then the tangential force component is defined separately in two cases: $\mathbf{F}_t = -k_t\delta\mathbf{s} - \gamma_t M_e \delta v_t$, for stick phase, and $\mathbf{F}_t = -\mu_{rr}F_n\mathbf{t}_{ij}$ for slip phase. During the slip phase the magnitude of $\mathbf{s}$ is adjusted to fulfill $|\mathbf{F}_t| = \mu_{rr}|F_n|$. Here $M_e = M/2$ is reduced mass for rod-rod collision, m is the mass of the rod, $\delta = d - r_{ij}$ and $v_n = \mathbf{v}_{ij}\cdot\mathbf{n}_{ij}$ are the overlap and relative velocity in the direction of normal, $\mathbf{n}_{ij} = (\mathbf{r}_i - \mathbf{r}_j)/r_{ij}$, while tangential direction $\mathbf{t}_{ij} = \mathbf{v}_t/v_t$ is specified by the relative tangential velocity $\mathbf{v}_t = \mathbf{v}_{ij} - v_n\mathbf{n}_{ij}$, μ_{rr} is coefficient of friction between rods. MD is performed in reduced units, all quantities are normalized by an appropriate combination of the diameter d, mass of virtual sphere m, and gravitation acceleration g. Typical values of material parameters are, $k_n = 5\ 10^6(mg/D)$,$k_t = 95k_n$, $\gamma_n = \gamma_t = 4\ 10^2(g/D)^{1/2}$. The coefficients of friction for rod-rod and rod-bottom collisions are $\mu_{rr} = 0.3$,$\mu_{rb} = 0.3$ respectively. Unless specified otherwise for interactions with walls we also used $\mu_{rw} = 0.3$.

To expedite the integration of Newton's equation we used simple leapfrog algorithm [14] with constant time step $\Delta t = 2.0\ 10^{-5}(d/g)^{1/2}$, however we tested that application of more accurate integration scheme such as 5^{th}-order Gear predictor-corrector did not introduce considerable changes.

Our choice of the values of material parameters is neither optimal for the comparison with experimental data nor unique. Because we observed very good agreement with the theoretical description for a single collision (see Fig. 12) we expect our algorithm to capture details of *short-term* collision with plate. However, for a long-term collision it may not be accurate.

APPENDIX B: DERIVATION OF REFLECTION COEFFICIENTS

Slip-stick. The stopping condition $u(t_1) = 0$ gives the total vertical impulse exerted by a plate on a rod for $0 < t < t_1$,

$$P_z(t_1) = u_0 \frac{mk^2}{\mu(k^2 + Z^2) + XZ} \tag{B1}$$

and correspondingly

$$P_x(t_1) = -u_0 \frac{m\mu k^2}{\mu(k^2 + Z^2) + XZ} \tag{B2}$$

Vertical velocity at the end of the contact

$$\begin{aligned} v_f &= v_1 + \frac{k^2 + X^2 + Z^2}{k^2 + Z^2}\int_{t_1}^{t_f} F_z = v_0 + \\ &+ \frac{k^2 + X^2 + \mu XZ}{\mu(k^2 + Z^2) + XZ}u_0 + \frac{k^2 + X^2 + Z^2}{m(k^2 + Z^2)}(P_z(t_f) - P_z(t_1)) \end{aligned} \tag{B3}$$

Assuming the kinematic restitution law $v_f = -\epsilon v_0$ and using (B1),(B2), we get

$$\begin{aligned} P_z(t_f) &= u_0 \frac{mk^2}{\mu(k^2 + Z^2) + XZ} \\ &- \left[v_0(1+\epsilon) + \frac{k^2 + X^2 + \mu XZ}{\mu(k^2 + Z^2) + XZ}u_0\right]\frac{m(k^2 + Z^2)}{k^2 + X^2 + Z^2} \end{aligned} \tag{B4}$$

$$\begin{aligned} P_x(t_f) &= -u_0 \frac{m\mu k^2}{\mu(k^2 + Z^2) + XZ} \\ &- \left[v_0(1+\epsilon) + \frac{k^2 + X^2 + \mu XZ}{\mu(k^2 + Z^2) + XZ}u_0\right]\frac{mXZ}{(k^2 + X^2 + Z^2)} \end{aligned} \tag{B5}$$

Now we can calculate the CM velocities after the contact. Substituting (B4),(B5) with $u_0 = c_x - \omega Z$ and $v_0 = c_z - V_z + \omega X$ into (10),(11), we get (18),(19).

Slip reversal. Using (5),(6 and the slip condition $F_x = \mu F_z$ for $t_1 < t < t_f$, we obtain the horizontal and vertical velocities at t_f,

$$u_f = \frac{\mu(k^2+Z^2)-XZ}{mk^2}(P_z(t_f)-P_z(t_1)) \quad \text{(B6)}$$

$$v_f = v_1 + \frac{k^2+X^2-\mu XZ}{mk^2}(P_z(t_f)-P_z(t_1)) \quad \text{(B7)}$$

Again assuming kinematic restitution condition $v_f = -\epsilon v_0$ and using (B1),(B2), we get for the impulse during the reversal phase

$$P_z(t_f) = u_0\frac{mk^2}{\mu(k^2+Z^2)+XZ} \quad \text{(B8)}$$
$$- \frac{mk^2}{k^2+X^2-\mu XZ}\left[(1+\epsilon)v_0 + \frac{k^2+X^2+\mu XZ}{\mu(k^2+Z^2)+XZ}u_0\right]$$

$$P_x(t_f) = -u_0\frac{\mu mk^2}{\mu(k^2+Z^2)+XZ} \quad \text{(B9)}$$
$$- \frac{\mu mk^2}{k^2+X^2-\mu XZ}\left[(1+\epsilon)v_0 + \frac{k^2+X^2+\mu XZ}{\mu(k^2+Z^2)+XZ}u_0\right]$$

The final horizontal velocity of CP

$$u_f = -\frac{\mu(k^2+Z^2)-XZ}{k^2+X^2-\mu XZ}\left[(1+\epsilon)v_0 + \frac{k^2+X^2+\mu XZ}{\mu(k^2+Z^2)+XZ}u_0\right] \quad \text{(B10)}$$

Substituting (B8),(B9) into (10)-(11), we get the CM velocities after the contact for the case of slip reversal

$$c_x' = u_0\left[1-\frac{\mu k^2}{\mu(k^2+Z^2)+XZ}\right]+\omega Z \quad \text{(B11)}$$
$$- \frac{\mu k^2}{k^2+X^2-\mu XZ}\left[(1+\epsilon)v_0 + \frac{k^2+X^2+\mu XZ}{\mu(k^2+Z^2)+XZ}u_0\right],$$

$$c_z' = v_0 + u_0\frac{k^2}{\mu(k^2+Z^2)+XZ} \quad \text{(B12)}$$
$$- \frac{k^2}{k^2+X^2-\mu XZ}\left[(1+\epsilon)v_0 + \frac{k^2+X^2+\mu XZ}{\mu(k^2+Z^2)+XZ}u_0\right] + V_z - \omega X$$

Substituting $u_0 = c_x - \omega Z$, $v_0 = c_z - V_z + \omega X$, we get (21),(22).